Escola de Primavera de Transição e Turbulência
Blumenau 2020

ABCM Associação Brasileira de Engenharia e Ciências Mecânicas

12th Spring School on Transition and Turbulence
September 21st-25th, 2020, Blumenau, SC, Brazil

EPTT-2020-0015
SAND EROSION OF ELBOWS IN SERIES ORIENTED IN TWO CONFIGURATIONS FOR MULTIPHASE FLOWS

Thiana A. Sedrez
Siamack A. Shirazi
The University of Tulsa, 800 S Tucker Dr, 74104, Tulsa, Oklahoma, USA
thiana-sedrez@utulsa.edu, siamack-shirazi@utulsa.edu

Abstract. *Erosion of elbows in series has received more attention recently as many facilities have elbows in series with various orientations and installations. It has been observed from experiments that, for liquid-dominated flows when the elbows are placed in series and with a small distance between them, the maximum erosion takes place in the second elbow. In this work, Computational Fluid Dynamics (CFD) studies are performed for liquid-solid flow to determine which configuration would softer more erosion: when the second elbow orientation is horizontal-vertical downward (Π-type) or horizontal-vertical upward (Z-type). Then, experiments were conducted with the liquid-gas-solid flow for the configuration chosen in the previous step. Finally, new CFD simulations are performed for the same operational conditions as the experiments. From the CFD simulations, it was found that the worst-case scenario would happen when the second elbow has orientation horizontal-vertical upward (Z-type). However, the liquid-gas-solid experiments showed that actually, erosion in the second elbow of the Z-type configuration is less than the erosion in the second elbow of the Π-type configuration and the liquid-gas-solid simulations corroborate the experimental results.*

Keywords: *elbows in series, erosion, liquid-solid flows, liquid-gas-solid flows*

1. INTRODUCTION

Studies of solid particle erosion in pipes, elbows, bends, plugged tees, gate valves, choke valves, cyclones separators and impeller of centrifugal pumps by various investigators in the past half-century is a confirmation that erosion is a significant problem in various industries and predicting erosion and all factors that contribute to erosion is a problem that is not well understood yet. Predicting erosion in elbows and pneumatic transport for the oil and gas and mining industries are the most studied topics. Moreover, the complexity of the flow inside specific geometries has increased either by the effect of geometry or the addition of another fluid phase. Elbows in series are examples of complex turbulent flows, where due to the curved walls of the elbows and centrifugal force, secondary vortices inside the elbows are generated that are making the upstream flow field more complex for the second elbow than in the first elbow.

Several studies of erosion in elbows in series are reported in the literature. For example, Kumar *et al.* (2014) performed experiments and Computation Fluid Dynamics (CFD) simulations to predict erosion in elbows in series in a 50.8 mm test loop using air-sand flow. Three elbows in series were used in the erosion loop to evaluate the effect of small particles on erosion ($75\ \mu m$) in carbon steel pipe material. In addition, four erosion models were tested. Overall, the first elbow presented a higher peak of erosion when compared to the second and third elbows. Experimental results showed that erosion takes place uniformly along the outer radius of the elbows with multiple highly eroded locations. The first elbow was the only one that presented erosion profile along the outer wall of the elbow with a single maximum erosion peak. Regarding the CFD simulations, in general, the erosion models over-predicted the maximum erosion value and shifted the maximum erosion location when compared to the experiments. This study shows how small particle erosion prediction can be challenging and may lead to erratic conclusions, especially when CFD simulations are undertaken, and care must be taken to ensure accurate simulation of these flows.

Felten (2014) only used numerical simulations to predict erosion in elbows in series in gas-solid as well. Here, the author changed the distance between the elbows and also the orientation between them. It was found that erosion in the first elbow is not affected by the distance or orientation between elbows. On the contrary, the erosion in the second elbow can be enhanced or reduced depending on the distance or angle between the elbows. However, erosion in the first elbow is higher than erosion in the second elbow for all cases investigated. In another study, Droubi *et al.* (2016) performed CFD simulations to predict the erosion of solid particles evaluating different geometrical parameters. One of the things the authors investigated was double bends, that is, elbows in series with different distances between the elbows. It is not clear in the paper if these particular simulations were performed with gas or liquid, however, the results show that the erosion in the second elbow is higher than the erosion in the first elbow for all cases studied. In addition, it was

observed that erosion in the first elbow decreases as the distance between the elbows is increased and that erosion in the second elbow increases as the distance between the elbows is increased. As can be seen from this short literature review, CFD simulations dominate the studies and, as already well known, can be a handy tool. However, there are still few experiments in the literature regarding elbows in series and some controversies have been observed in the numerical simulations. Thus, the purpose of this study is to evaluate erosion of elbows in series with different orientations between the elbows for stainless steel (SS316) pipe material, liquid-solid and liquid-gas-solid flows. Therefore, two geometries are considered and the results are compared with the experimental data for validation purposes.

2. METHODOLOGY

CFD simulations were performed in liquid-solid flow to examine the worse combination of elbows in series for erosion severity. A preliminary study was conducted with three geometries, however, the results of two configurations will be shown in this work. The numerical approach adopted for the liquid-solid simulations was the Euler-Lagrange method, and the liquid-gas-solid was the Euler-Euler-Lagrange approach with gas bubble size of 0.55 mm (Sedrez and Shirazi, 2020). All numerical simulations are conducted by the commercial CFD code ANSYS Fluent 17.2. The fluid flow was calculated based on the Euler approach using the Reynolds time-averaged Navier-Stokes (RANS) equations with the differential Reynolds stress turbulence model (RSM). The RANS equations used to represent the fluid field can be found as follow:

$$\frac{\partial}{\partial t}(\alpha_q\,\rho_q) + \boldsymbol{\nabla}\cdot(\alpha_q\,\rho_q\,\mathbf{v}_q) = 0 \tag{1}$$

and

$$\frac{\partial}{\partial t}(\alpha_q\,\rho_q\,\mathbf{v}_q) + \boldsymbol{\nabla}\cdot(\alpha_q\,\rho_q\,\mathbf{v}_q\,\mathbf{v}_q) = -\,\alpha_q\,\boldsymbol{\nabla} p \,-\, \boldsymbol{\nabla}\cdot(\boldsymbol{T^V} + \boldsymbol{T^R}) \,+\, \alpha_q\,\rho_q\,\boldsymbol{g} + \boldsymbol{F}\,, \tag{2}$$

where α_q is the phase volume fraction, ρ_q is the phase density, $\mathbf{v}_q$ is the phase velocity vector, and $\boldsymbol{F}$ is the source term. From Equation (2), the viscous stress ($\boldsymbol{T^V}$) can be represented by Newton's law of viscosity for Newtonian fluids (Bird *et al.*, 2004). The Reynolds tensor ($\boldsymbol{T^R}$) is generated as a result of the application of the averaging procedure. This additional term appearing in the temporal averaged equations, related to floating quantities, represents the effect of the turbulence and needs to be modeled. The expression is written as:

$$\boldsymbol{T^R} = \rho_f\,\overline{\mathbf{v}'_f\,\mathbf{v}'_f}\,. \tag{3}$$

The Reynolds Stress Model (RSM) is used to resolve the flow turbulence because it is indicated to very swirl flows and can to predict secondary flows in elbows, and the main equation is:

$$\frac{\partial}{\partial t}\left(\rho_f\,\overline{\mathbf{v}'_f\,\mathbf{v}'_f}\right) \,+\, \boldsymbol{\nabla}\cdot\mathbf{v}_f\,\left(\rho_f\,\overline{\mathbf{v}'_f\,\mathbf{v}'_f}\right) = \boldsymbol{\Psi} \,+\, \boldsymbol{\Pi} \,-\, \boldsymbol{\epsilon} \,+\, \boldsymbol{D}_T \,+\, \boldsymbol{D}_M\,, \tag{4}$$

where $\boldsymbol{\Psi}$ is the stress production term, $\boldsymbol{\Pi}$ is the pressure strain term (Launder *et al.* (1975)), ϵ is dissipation term, $\mathbf{D_T}$ is the turbulent diffusion term, and $\mathbf{D_M}$ is the molecular diffusion term. In this model, $\boldsymbol{\Pi}$, ϵ, and $\mathbf{D_T}$ need to be modeled to close the equation.

In a Lagrangian reference frame, particle trajectories are calculated by integrating a force balance on the particle. The forces which were considered in this work include particle inertia, gravitational, buoyancy, drag, virtual mass for liquid-solid flow, and the pressure gradient force is also added for liquid-gas-solid flows as discussed by Sedrez and Shirazi (2020). The equation of particle motion is given by:

$$\frac{d\mathbf{v}_p}{dt} \,=\, \frac{18\,\mu_f}{\rho_p\,d_p^2}\,\frac{C_d\,Re_p}{24}\,(\mathbf{v}_f \,-\, \mathbf{v}_p) \,+\, C_{vm}\,\frac{\rho_f}{\rho_p}\,\left(\mathbf{v}_p\,\nabla\,\mathbf{v}_f \,-\, \frac{d\mathbf{v}_p}{dt}\right) \,+\, \frac{\rho_f}{\rho_p}\,\mathbf{v}_p\,\nabla\,\mathbf{v}_f \,+\, \left(\frac{\rho_p \,-\, \rho_f}{\rho_p}\right)\,\mathbf{g}\,, \tag{5}$$

where, in the above equations, $\mathbf{v}_p$ and $\mathbf{v}_f$ are the particles and fluid velocities, respectively, ρ_p and ρ_f are the particle and fluid density, μ_f is the fluid viscosity, d_p is the particle diameter, C_d is the drag coefficient, Re_p is the particle Reynolds number, and C_{vm} is the virtual mass factor (0.5). In this work, the non-spherical drag coefficient proposed by Haider and Levenspiel (1989) is used with a shape factor of 0.8. The coefficient for the drag law (C_d) was calculated from Equation (6):

$$C_D = \frac{24}{Re_{sph}}\,\left(1 \,+\, b_1\,Re_{sph}^{b_2}\right) \,+\, \frac{b_3\,Re_{sph}}{b_4 \,+\, Re_{sph}}\,, \tag{6}$$

where b_1, b_2, b_3, and b_4 are constants based on the particle sphericity to account for particle shape given by Haider and Levenspiel (1989). Particles are assumed as dilute and the particle-wall rebound model used in the simulations was proposed by Grant and Tabakoff (1975), as follow:

$$e_n = 0.993 - 1.76\alpha + 1.56\alpha^2 - 0.49\alpha^3 \tag{7}$$

and

$$e_t = 0.988 - 1.66\alpha + 2.11\alpha^2 - 0.67\alpha^3\,, \tag{8}$$

where α is the impact angle, and e_n and e_t are the normal and tangential components of the rebound model, respectively.

In a preliminary study, both the Arabnejad *et al.* (2015) and Oka *et al.* (2005); Oka and Yoshida (2005) erosion model were tested. The Arabnejad model is more conservative as compared to the Oka model, and in this work, the erosion results are shown for Oka model. Oka *et al.* (2005); Oka and Yoshida (2005) developed an erosion model that can be written as:

$$ER = 1.0 \times 10^{-9}\, \rho_w\, k_0\, f(\alpha)\, (Hv)^{k_1}\, \left(\frac{u_p}{V'}\right)^{k_2}\, \left(\frac{d_p}{d'}\right)^{k_3} \tag{9}$$

and

$$f(\alpha) = (\sin\alpha)^{n_1}\, [\,1\, +\, Hv\,(1\, -\, \sin\alpha)]^{n_2}\,, \tag{10}$$

where ρ_w is the target material density, Hv is the Vickers hardness of the target material, d_p is the particle diameter, d' is the reference diameter, V' is the reference impact speed of the reference particle, and the other constants are given as follow: k_0 = 65, k_1 = - 0.12, $k_2 = 2.3(Hv)^{0.038}$, k_3 = 0.19, $n_1 = 0.71(Hv)^{0.14}$, $n_2 = 2.4(Hv)^{-0.94}$, d' = 326 μm and V' = 104 m/s.

The two geometries evaluated can be found in Figs. 1 (a) and (b). Each one of them has 42 diameters straight vertical pipe before the first elbow. The distance between the first and second elbow is three diameters. The pipe diameter is 50.8 mm and the elbows are standard, that is, the curvature is R/D = 1.5.

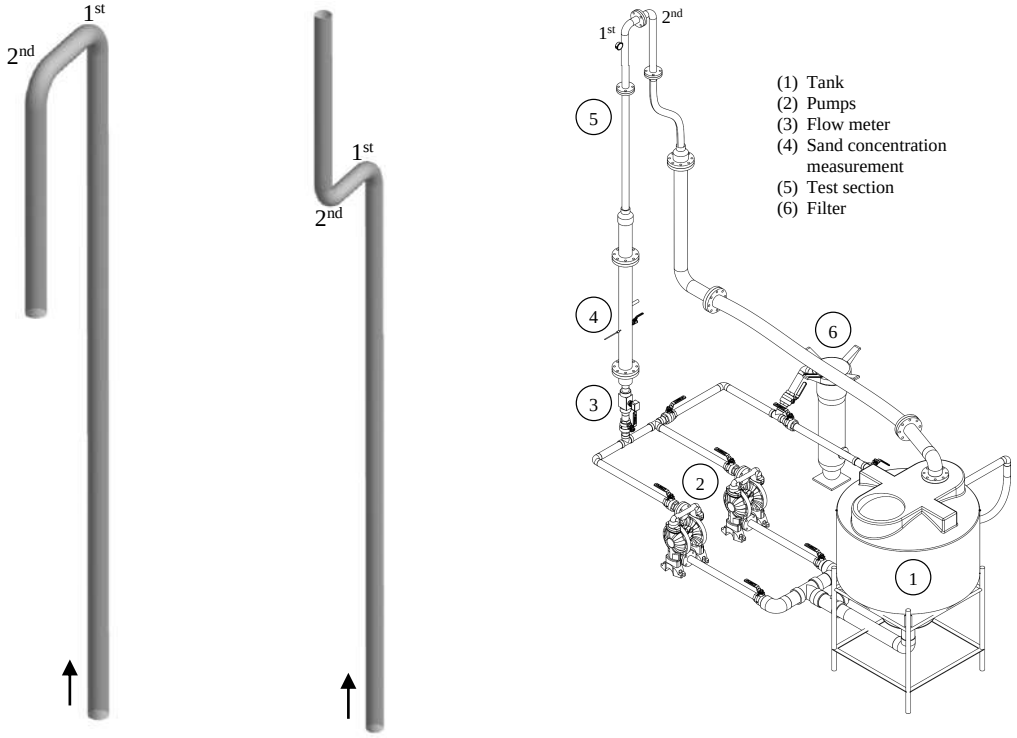

(a) Π-type (Case 1) (b) Z-type (Case 2) (c) Schematic of the experiemntal facility

Figure 1: Geometries used in the simulations and experimental facility.

For Π-type configuration, the first elbow orientation is upward vertical-to-horizontal, while the second elbow orientation is horizontal-to-vertical downward. Z-type configuration presents the orientation of the second elbow 90° to the second elbow of Π-type, and it is characterized by horizontal-to-horizontal orientation.

The mesh study was done for Π-type and can be found in more detail in Sedrez *et al.* (2019, 2018a,b). The method used consists of a statistical evaluation of the variable chosen to be tested based on the Richardson extrapolation, called the grid convergence index method (GCI). As a result, the method presents the discretization error of the mesh for erosion. In this case, the error of discretization is 3.4%. The variable chosen for the study was erosion rate (mm/day), and for

the method, three meshes were created with the same growth ratio between them in all directions (approximately 1.3). The methodology calculates an extrapolated value and indicates if there is monotonic convergence for the global variable tested. In the end, the mesh that is going to be used for further simulations has to be in the asymptotic range of the monotonic convergence. The details of the final mesh used for the simulations can be found in Figure 2, which has 351768 elements and first layer thickness of 300 μm.

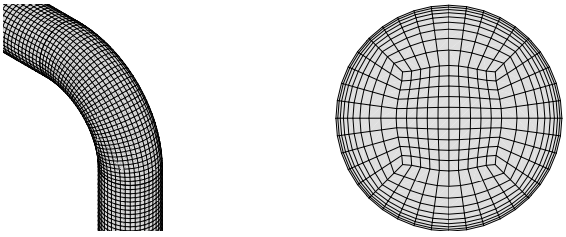

(a) Elbow detail (b) Cross-section

Figure 2: Mesh used in the simulations.

Therefore, the same operational conditions used for the experiments were applied to all numerical simulation cases. The boundary conditions used were velocity-inlet at the inlet of the 50.8 mm diameter vertical pipe and pressure-outlet at the outlet of the geometry. The fluid is water and air (when applicable), and particles are sand with a density of 2,650 kg/m^3. The fluid field was considered steady-state as well as the particles for liquid-solid flow and transient for liquid-gas-solid flow. The same amount of particles were released into the domain for all cases (about 100,000 particles). The number of particles also was further increased and the results did not change.

Experiments were performed for both configurations for liquid-gas-solid flow, however, only the Π-type is performed for liquid-solid flow. The flow loop used in this study can be found in Fig. 1 (c). Sand is mixed with water in 1135 liters conical bottom tank and pumped through the test section by two air-operated diaphragm pumps. Before the test section, there is a 50.8 mm of diameter vertical pipe section where liquid velocity is measured, followed by a 101.6 mm of diameter pipe section where sand concentration is measured. The facility also has a bypass line with a filter to filter all the sand after each day (approximately 6 hours) of the experiment is conducted. The experimental conditions for the liquid-solid case are the fluid velocity of 7 m/s and the particle size of 300 μm. The particle volume concentration is 1%. The duration of the experiment was about 16 hours and sand was replaced three times during the experiment with fresh sand, although our previous study has shown that sand size remains unchanged during each about 6 hours of the experiment. For liquid-solid flow, particle size and concentration are the same as the previous case, however, water and air superficial velocities are approximately 5.5 m/s, and the duration of each experiment was about 4 hours.

3. COMPUTATIONAL FLUID DYNAMICS RESULTS

Figure 3 shows the maximum predicted erosion rate results for liquid-solid flow for both configurations and the comparison with experiments for the Π-type configuration. It is possible to observe that CFD agrees well with the experiment. The maximum erosion ratio of the second elbow to the first elbow is 1.72 for the experiment. That means that the maximum erosion in the second elbow is 72% higher than the maximum erosion in the first elbow. CFD simulations are showing that the maximum erosion ratio of the second to the first elbow is 1.69. Additionally, the Z-type configuration shows that erosion in the second elbow would be 3.08 times the erosion in the first elbow. For liquid-solid flows, the Z-type would be the worse configuration of elbows in series for the distance between elbows tested. In this case, CFD is over-predicting erosion by 60%.

Figure 4 presents the erosion contour for the CFD simulations. Here, erosion is expressed as erosion flux ($kg/m^2.s$). It is possible to observe the similarity of the erosion contour between Figs. 4 (a) and (b), besides the difference in the erosion magnitude. Both present maximum erosion located toward the end of the elbow outer radii and with similar erosion patterns.

Figure 5 presents the experimental and numerical results for liquid-gas-solid flows. The experimental results show that the Z-type configuration decreases the erosion in the second elbow as compared with the Π-type configuration, which is the opposite of what was predicted for the liquid-solid flow. The reduction is about 45%. The same behavior can be found in the CFD simulations. Additionally, the numerical results are in excellent agreement with the experiments.

4. CONCLUSIONS

In this study, CFD simulations of two geometries with different configurations of elbows in series were performed. The simulation results were compared with the experimental data for validation, and the main conclusions are as follows. The predicted erosion with Eulerian-Eulerian-Lagrangian model utilized here is in excellent agreement (within 8% which is nearly within the uncertainty of the data) with the experimental data for both configurations. The maximum erosion

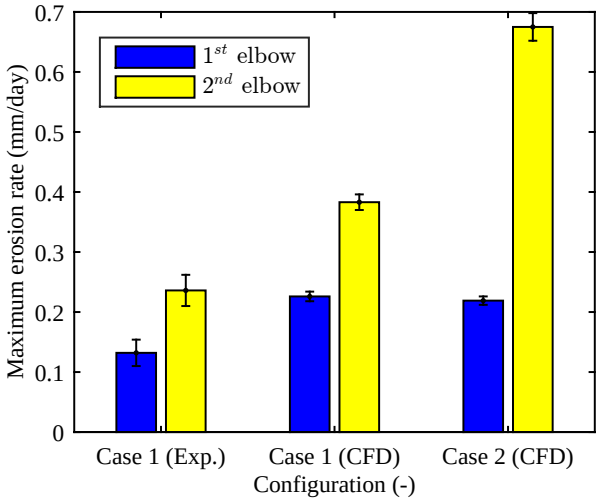

Figure 3: Maximum erosion rate for liquid-solid flow.

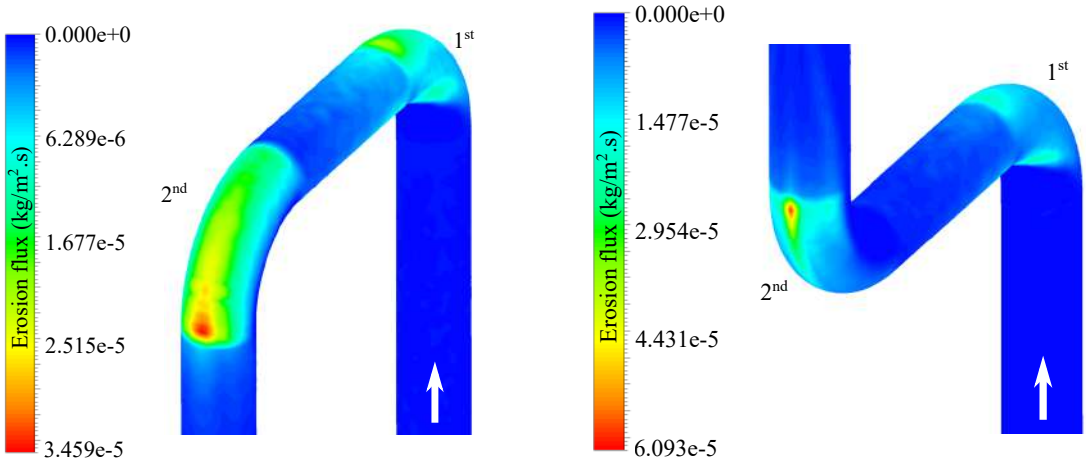

(a) Π-type (Case 1) (b) Z-type (Case 2)

Figure 4: Erosion contour for liquid-solid flow.

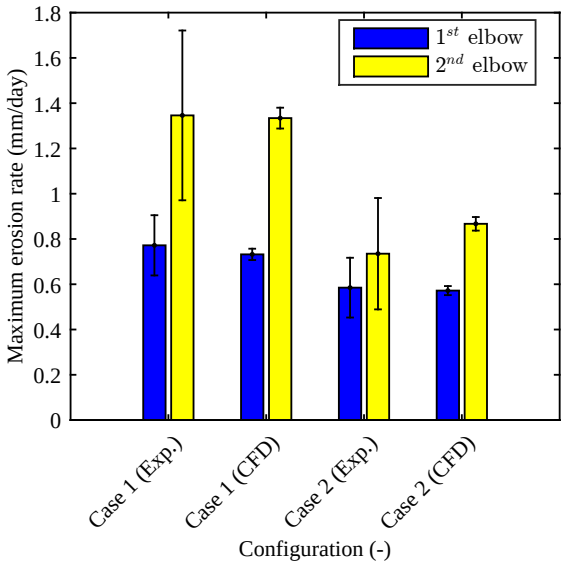

Figure 5: Comparison of CFD and experiments for liquid-gas-solid flow.

location for both elbows is experimentally observed to be at the end of the elbow curvature, and the same is observed in the CFD simulations. The worst scenario found was the second elbow of the Z-type configuration. Thus, this combination of elbow orientation should be avoided in the design of piping systems when the presence of solids in liquid are anticipated. However, for liquid-gas-solid flow, the Π-type orientation is still the worse combination of elbows in series.

5. ACKNOWLEDGEMENTS

The authors would like to thank Petrogal/CNPq process number 201530/2016-3 for the support of this research and also the support of the Erosion/Corrosion Research Center (E/CRC) member companies.

6. REFERENCES

Arabnejad, H., Mansouri, A., Shirazi, S.A. and McLaury, B.S., 2015. "Development of mechanistic erosion equation for solid particles". *Wear*, Vol. 332-333, pp. 1044–1050.

Bird, R.B., Stewart, W.E. and Lightfoot, E.N., 2004. *Transport phenomena*. Wiley, New York, 2nd edition.

Droubi, M.G., Tebowei, R., Islam, S.Z., Hossain, M. and Mitchell, E., 2016. "Computational Fluid Dynamic Analysis of Sand Erosion in 90 o Sharp Bend Geometry". *Ninth International Conference on Computational Fluid Dynamics*, pp. 1–9.

Felten, F.N., 2014. "Numerical prediction of solid particle erosion for elbows mounted in series". In *4th Joint US-European Fluids Engineering Division Summer Meeting - ASME*. pp. 1–10.

Grant, G. and Tabakoff, W., 1975. "Erosion prediction in turbomachinery resulting from environmental solid particles". *Journal of Aircraft*, Vol. 12, No. 5, pp. 471–478.

Haider, A. and Levenspiel, O., 1989. "Drag Coefficient and Terminal Velocity of Spherical and Nonspherical Particles". *Powder Technology*, Vol. 58, pp. 63–70.

Kumar, P., Smith, B., Vedapuri, D., Subramani, H.J. and Rhyne, L.D., 2014. "Sand Fines Erosion in Gas Pipelines – Experiments and CFD Modeling". In *Corrosion 2014*. San Antonio, 3964, pp. 1–12.

Launder, B.E., Reece, G.J. and Rodi, W., 1975. "Progress in the development of a reynolds-stress turbulence closure". *Journal of fluid mechanics*, Vol. 68, No. 3, pp. 537–566.

Oka, Y.I., Okamura, K. and Yoshida, T., 2005. "Practical estimation of erosion damage caused by solid particle impact. Part 1 : Effects of impact parameters on a predictive equation". *Wear*, Vol. 259, No. 1-6, pp. 95–101.

Oka, Y.I. and Yoshida, T., 2005. "Practical estimation of erosion damage caused by solid particle impact. Part 2: Mechanical properties of materials directly associated with erosion damage". *Wear*, Vol. 259, No. 1-6, pp. 102–109.

Sedrez, T.A., Rajkumar, Y.R., Shirazi, S.A., Khanouki, H.A. and McLaury, B.S., 2018a. "CFD Predictions and Experiments of Erosion of Elbows in Series in Liquid Dominated Flows". In *5th Joint US-European Fluids Engineering Summer Conference - ASME*. Montreal, Quebec, Canada.

Sedrez, T.A., Rajkumar, Y.R., Shirazi, S.A., Sambath, K. and Subramani, H.J., 2018b. "CFD simulations and experiments of sand erosion for liquid dominated multiphase flows in an elbow". In *Proceedings of the 11th North American Conference on Multiphase Production Technology*. Banff, Alberta, Canada, pp. 1–12.

Sedrez, T.A. and Shirazi, S.A., 2020. "Erosion of elbows in series for liquid-dominated multiphase flows: a CFD and experimental analysis". *Multiphase Science and Technology*, p. Forthcoming Article.

Sedrez, T.A., Shirazi, S.A., Rajkumar, Y.R., Sambath, K. and Subramani, H.J., 2019. "Experiments and CFD simulations of erosion of a 90° elbow in liquid-dominated liquid-solid and dispersed-bubble-solid flows". *Wear*, Vol. 426-427, pp. 570–580.

7. RESPONSIBILITY NOTICE

The authors are the only responsible for the printed material included in this paper.